Journal of Ginseng Research 46 (2022) 738–749

Contents lists available at ScienceDirect

Journal of Ginseng Research

journal homepage: https://www.sciencedirect.com/journal/journal-of-ginseng-research

Research Article

Ginsengenin derivatives synthesized from 20(*R*)-panaxotriol: Synthesis, characterization, and antitumor activity targeting HIF-1 pathway

Hong-Yan Guo [a, 1], Yue Xing [a, 1], Yu-Qiao Sun [a], Can Liu [a], Qian Xu [a], Fan-Fan Shang [a], Run-Hui Zhang [a], Xue-Jun Jin [a], Fener Chen [b], Jung Joon Lee [a], Dongzhou Kang [a, *], Qing-Kun Shen [a, *], Zhe-Shan Quan [a, *]

[a] *Key Laboratory of Natural Medicines of the Changbai Mountain, Ministry of Education, College of Pharmacy, Yanbian University, Yanji, Jilin, China*
[b] *Engineering Center of Catalysis and Synthesis for Chiral Molecules, Department of Chemistry, Fudan University, Shanghai, China*

ARTICLE INFO

Article history:
Received 2 July 2021
Received in revised form
26 January 2022
Accepted 8 March 2022
Available online 10 March 2022

Keywords:
20(*R*)-Panaxotriol
Antitumor
Derivatives
HIF-1α

ABSTRACT

Background: Ginseng possesses antitumor effects, and ginsenosides are considered to be one of its main active chemical components. Ginsenosides can further be hydrolyzed to generate secondary saponins, and 20(*R*)-panaxotriol is an important sapogenin of ginsenosides. We aimed to synthesize a new ginsengenin derivative from 20(*R*)-panaxotriol and investigate its antitumor activity *in vivo* and *in vitro*.
Methods: Here, 20(*R*)-panaxotriol was selected as a precursor and was modified into its derivatives. The new products were characterized by ^{1}H-NMR, ^{13}C-NMR and HR-MS and evaluated by molecular docking, MTT, luciferase reporter assay, western blotting, immunofluorescent staining, colony formation assay, EdU labeling and immunofluorescence, apoptosis assay, cells migration assay, transwell assay and *in vivo* antitumor activity assay.
Results: The derivative with the best antitumor activity was identified as 6,12-dihydroxy-4,4,8,10,14-pentamethyl-17-(2,6,6-trimethyltetrahydro-2*H*-pyran-2-yl)hexadecahydro-1*H*-cyclopenta[a]phenanthren-3-yl(*tert*-butoxycarbonyl)glycinate (**A11**). The focus of this research was on the antitumor activity of the derivatives. The efficacy of the derivative **A11** (IC_{50} < 0.3 μM) was more than 100 times higher than that of 20(*R*)- panaxotriol (IC_{50} > 30 μM). In addition, **A11** inhibited the protein expression and nuclear accumulation of the hypoxia-inducible factor HIF-1α in HeLa cells under hypoxic conditions in a dose-dependent manner. Moreover, **A11** dose-dependently inhibited the proliferation, migration, and invasion of HeLa cells, while promoting their apoptosis. Notably, the inhibition by **A11** was more significant than that by 20(*R*)-panaxotriol ($p < 0.01$) *in vivo*.
Conclusion: To our knowledge, this is the first study to report the production of derivative **A11** from 20(*R*)-panaxotriol and its superior antitumor activity compared to its precursor. Moreover, derivative **A11** can be used to further study and develop novel antitumor drugs.

1. Introduction

Cancer can be described as the uncontrolled growth and spread of abnormal cells, which can also affect other body parts and may spread to other organs. Etiology and pathogenesis of tumor are not fully understood. Tumor may act as a leading trigger for death worldwide [1], with its incidence increasing every year [2]. The discovery of cancer drugs has presented a significant challenge for the scientific community due to the challenges associated with evaluating and verifying various possible targets [3]. Globally, cervical cancer is the fourth most common cancer amongst women,

Abbreviations: HIF-1, hypoxia-inducible factor-1; DMEM, Dulbecco's modified Eagle's medium; FBS, fetal bovine serum; VEGF, vascular endothelial growth factor; Bcl-2, B cell lymphoma-2; Bax, Bcl-2-associated X; GAPDH, glyceraldehyde 3-phosphate dehydrogenase; MMP, matrix metalloproteinase; Topo, topoisomerase; TLC, thin-layer chromatography; HR-MS, high-resolution mass spectra; OD, optical density; PBS, phosphate-buffered saline; EdU, 5-ethynyl-2'-deoxyuridine.

* Corresponding authors. Key Laboratory of Natural Medicines of the Changbai Mountain, Ministry of Education, College of Pharmacy, Yanbian University, Yanji, Jilin, 133002, China.
E-mail addresses: kangdz@ybu.edu.cn (D. Kang), qkshen@ybu.edu.cn (Q.-K. Shen), zsquan@ybu.edu.cn (Z.-S. Quan).
[1] Hong-Yan Guo and Yue Xing contributed equally to this work.

https://doi.org/10.1016/j.jgr.2022.03.001

ranking only after breast cancer (2.1 million cases), colorectal cancer (0.8 million) and lung cancer (0.7 million). Globally, the average age at diagnosis of cervical cancer was 53 years, and the global average age at death was 59 years [4].

A lack of oxygen is the central feature of many solid tumors. Tumor cells grow rapidly in the body, compress blood vessels, and cause hypoxia in body tissues [5,6]. In the hypoxic microenvironment, hypoxia-inducible factor-1 (HIF-1) acts as a regulatory factor in the transcription process and promotes the occurrence and development of tumors. In consequence, HIF-1 proved to be pivotal anti-cancer drug mark [7–9]. HIF-1α and HIF-1β constitute the heterodimeric transcription factor HIF-1 [10]. The level of HIF-1α is strictly controlled by the concentration of oxygen in the cell, but the level of HIF-1β is not influenced by the oxygen content [11]. HIF-1α regulates the spread, migration and production of tumor cells [12], and there is a positive correlation between the cellular concentration of HIF-1α and the severity of cancer [13]. In addition, cancer recurrence after resection is related to overexpression of HIF-1α [14]. Therefore, HIF-1α has been used as an effective target for working on new antitumor medicine [15–17].

Ginseng, a herbal supplement, has cardioprotective, antitumor, anti-ischemic shock, anti-arrhythmia, anti-myocardial ischemia, anti-inflammatory, anti-apoptotic and antioxidant effects [18–20]. Among its chemical components, ginsenosides are considered one of the main active components [21,22]. Ginsenosides can be hydrolyzed to generate secondary sapogenins. Among them, 20(*R*)-panaxotriol (Fig. 1) is an important sapogenin of ginsenosides [23]. Several studies have shown that the potential antitumor effect of panaxotriol on DU-15 cells is adjusted by sub-G1 cell cycle arrest, cell migration repression, and mitochondrial-mediated apoptosis [24]. In addition, Li et al. evaluated the inhibitory effects of panaxotriol derivatives on K562/ADR, Du-145, HeLa, MCF-7, and HepG2 cell lines. It has been proven that panaxotriol can selectively inhibit the human leukemia progenitor K562/ADR by arresting the cell cycle [25].

Many drugs containing 1,2,3-triazole stents are used clinically, including TSAO [26] (anti-HIV drugs), ceftazidime [27] (antibiotics), CAI [28] (anti-cancer drugs), and azoles Batan [29] (antibacterial agent). In addition, there are many studies on the biological activity of the structure containing triazoles [30–37]. 1,2,3-triazole has become a powerful pharmacophore. In terms of biological activity, they are considered essential structural fragments and exist in many natural drug derivatives with antitumor activity [38–40]. Furthermore, these functionality structural fragments, containing cinnamic acid [41,42], carbamates [43,44], and amino acids [45], are extensively present in numerous molecule which have biological activity and exhibit more antitumor properties.

Based on the principle of drug combination and the above findings, we designed and synthesized four new 20(*R*)-panaxotriol derivatives by attaching these pharmacophores to the C-3 or C-6 position of panaxotriol. The anti-proliferative activity of the target compound against human hepatoma cancer (Hep3B) was evaluated. In addition, we selected the derivative **A11** (Fig. 1) with the strongest anti-proliferative activity, studied its possible mechanism of action of HIF-1, and particularly focused on the activity of this panaxotriol derivative on cell apoptosis and cell migration. Finally, we conducted *in vivo* experiments to verify its antitumor properties.

2. Materials and methods

2.1. Materials

20(*R*)-panaxotriol was obtained from Nanjing Dilger Medical Technology Co.Ltd. All organic reagents used for the experiment were analytically pure, and other chemicals were purchased from Aladdin reagent. Hep3B cells and HeLa cells were obtained from American Type Culture Collection (ATCC, Manassas, VA, USA) and were cultured in Dulbecco's modified Eagle's medium (DMEM) with 10% heat-inactivated fetal bovine serum (FBS, Hyclone, Logan, UT, USA), penicillin (100 U/mL), and streptomycin (100 U/mL) (Invitrogen, Carlsbad, CA, USA). The hypoxic culture was kept in a gas-controlled chamber (Thermo Electron Corp., Marietta, OH, USA) and maintained at 37 °C under 5% CO_2, 94% N_2, and 1% O_2. Antibodies against the hypoxia-inducible factor (HIF)-1α were purchased from BD Biosciences (San Diego, CA, USA). Antibodies against the vascular endothelial growth factor (VEGF), matrix metalloproteinase (MMP)-9, HIF-1β, B cell lymphoma-2 (Bcl-2), Bcl-2-associated X (Bax), glyceraldehyde 3-phosphate dehydrogenase (GAPDH), and topoisomerase (Topo)-I were obtained from Santa Cruz Biotechnology (Santa Cruz, CA, USA). Antibodies against cleaved Caspase-3 were purchased from Cell Signaling Technology. Other cell culture reagents were obtained from commercial companies (UNIV, Shanghai, China; Huayi Biotechnology Co., Ltd, Changchun, China).

2.2. Synthesis of 20(R)-panaxatriol derivatives

2.2.1. Procedure for the preparation of compounds *A1-A3*, *B1-B3*, and *C1-C3*

First, 20(*R*)-panaxotriol (0.4 mmol, 190 mg) was mixed with toluene (5 mL) in an ice bath and slowly different substituted isocyanates (0.8 mmol) and triethanolamine (110 μL, 0.24 mmol) were added. Then stirred for 24h at 100 °C under nitrogen protection. The crude compounds were obtained by evaporating the solvent after thin-layer chromatography (TLC), confirming the completion of the reaction. The desired compounds were purified by silica gel column chromatography (dichloromethane/methanol, 100:1-50:1 v/v).

2.2.2. Procedure for the preparation of compounds *A4-A12*, *B4-B12*, and *C4-C12*

First, 20(*R*)-panaxotriol (0.4 mmol, 190 mg) was mixed with different carboxyl compounds (1.2 mmol), N-ethyl-N′-(3-(dimethylamino) propyl) carbodiimide (1.2 mmol) and 4-(dimethylamino)pyridine (0.4 mmol) in CH_2Cl_2 (5 mL) at 37 °C, and stirred for 24 h. After TLC confirmed the end of the reaction, it was poured into water (10 mL) and extracted three times with dichloromethane (3 × 10 mL); the organic phase was washed with water (1 × 10 mL) and saturated NaCl (1 × 10 mL), and dried over Na_2SO_4 to obtain crude compounds. The desired compounds were purified by silica gel column chromatography (dichloromethane/methanol, 200:1-50:1 v/v).

2.2.3. Procedure for the preparation of compounds *A13-A15*

The mixture of compounds **A10**-**A12** (50 mg) and 200–300 mesh silicone (150 mg) was stirred in 2 mL of toluene at 120 °C for 6 h. The crude compounds were obtained by evaporating the solvent after TLC, confirming the completion of the reaction. The desired compounds were then purified by silica gel column chromatography (dichloromethane/methanol, 100:1-30:1 v/v).

2.3. Analysis of 20(R)-panaxatriol derivatives

Silica gel plate GF254 was used for TLC analysis to detect the reaction. The instrument used for the ^{1}H-NMR and ^{13}C-NMR spectroscopic analyses of all compounds was: AV-300 (Bruker BioSpin, Switzerland), with $CDCl_3$ as the solvent and trimethylsilane as the interior label. The coupling constant is expressed in Hz, and the chemical shift is indicated in ppm. The high-resolution

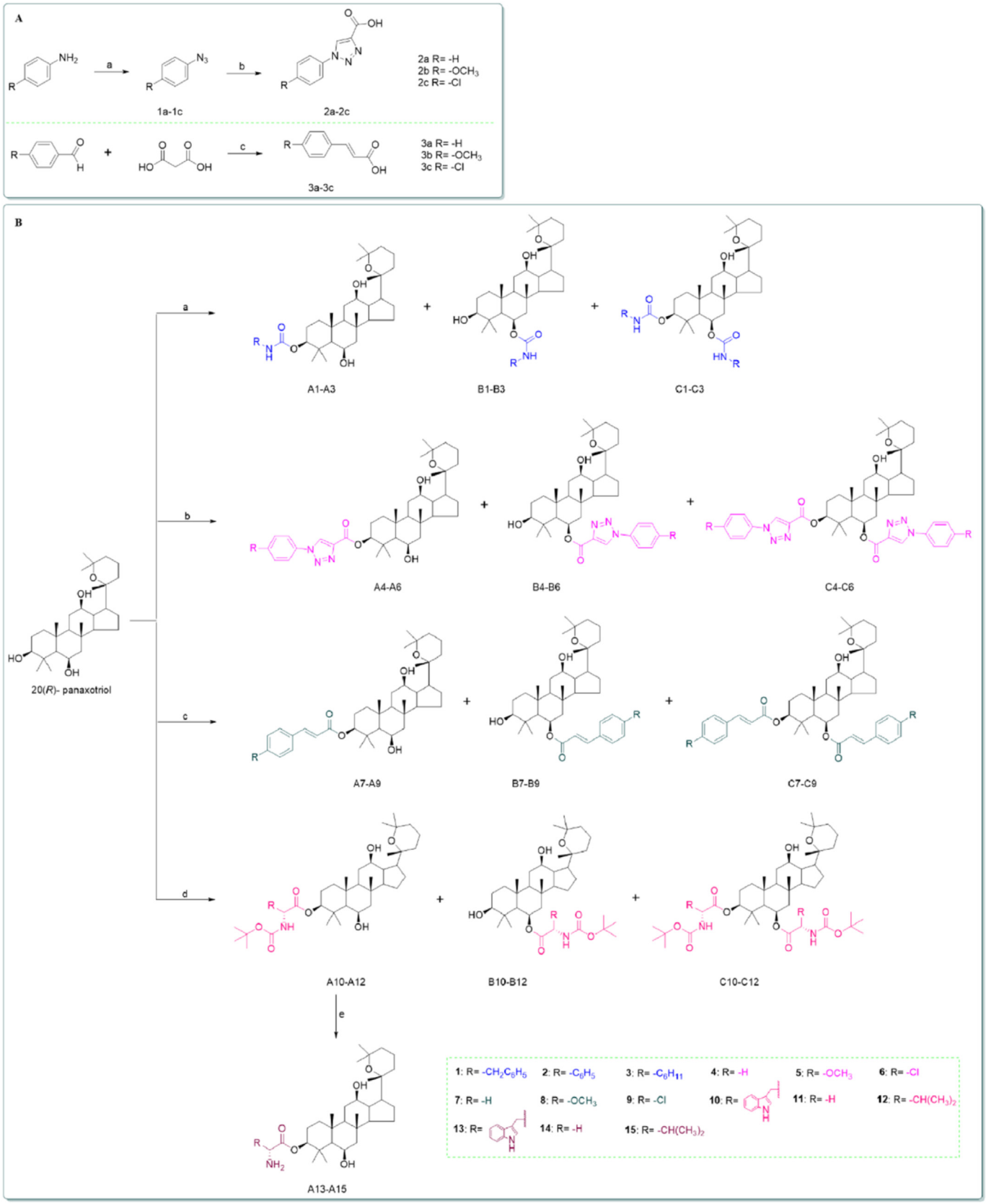

Fig. 1. Reagents and conditions: (**A**) (a) (i) 10% HCl, $NaNO_2$, H_2O, 0–5 °C, 30 min; (ii) NaN_3, H_2O, 0–5 °C, 2–4 h. (b) propiolic acid, L-ascorbic acid sodium salt, $CuSO_4 \cdot 5H_2O$, *n*-BuOH/H_2O, r.t., 24 h. (c) pyridine in DMF, 90 °C, 6 h. (**B**) (a) different substituted isocyanates, TEA, methylbenzene, 100 °C, 24 h. (b) **2a**-**2c**, EDC, DMAP, CH_2Cl_2, 37 °C, 24 h. (c) **3a**-**3c**, EDC, DMAP, CH_2Cl_2, 37 °C, 24 h. (d) different amino acids with *t*-butoxycarbonyl, EDC, DMAP, CH_2Cl_2, 37 °C, 24 h. (e) silica gel column chromatography, methylbenzene, 120 °C, 6 h.

mass spectra (HR-MS) were analyzed using electrospray ionization (ESI) on a Thermo Scientific LTQ Orbitrap XL spectrometer.

The Compound, 6,12-dihydroxy-4,4,8,10,14-pentamethyl-17-(2,6,6-trimethyltetrahydro-2*H*-pyran-2-yl)hexadecahydro-1*H*-cyclopenta[a]phenanthren-3-yl(*tert*-butoxycarbonyl)glycinate (**A11**) was further characterized using physical and spectral data. (Spectra of other 20(*R*)-panaxatriol derivatives are included in the Supporting Materials). White powder; Mp: 233-234 °C; yield 52%. ^{1}H-NMR ($CDCl_3$, 300 MHz, ppm): δ 6.28 (s, 1H, OH-12), 5.09-5.01 (m, 1H, −NH−), 4.55-4.50 (m, 1H, CH-3), 4.15-4.06 (m, 1H, CH-6), 3.91 (d, J = 4.9 Hz, 2H, $-CH_2$-C═O), 3.53 (td, J = 10.1, 5.0 Hz, 1H, CH-12), 1.98-1.51 (m, 15H, panaxotriol-H), 1.45 (s, 9H, $-C(CH_3)_3$), 1.41-1.32 (m, 3H, panaxotriol-H), 1.26 (s, 3H, panaxotriol-CH_3), 1.22 (s, 3H, panaxotriol-CH_3), 1.18 (s, 6H, panaxotriol-CH_3), 1.13-1.11 (m, 2H, panaxotriol-H), 1.06 (s, 6H, panaxotriol-CH_3), 1.00 (s, 1H, panaxotriol-H), 0.96 (s, 3H, panaxotriol-CH_3), 0.90 (s, 3H, panaxotriol-CH_3), 0.87-0.81 (m, 1H, panaxotriol-H). ^{13}C-NMR ($CDCl_3$, 75 MHz, ppm): δ 170.18, 155.61, 82.06, 79.86, 77.24, 73.15, 69.72, 68.34, 61.10, 54.64, 50.99, 49.29, 48.76, 47.11, 42.66, 40.96, 38.99, 38.29, 36.41, 35.70, 33.01, 31.08, 30.72, 30.40, 29.68, 28.33 (3C), 27.15, 25.11, 23.37, 19.39, 17.23, 17.16, 17.01, 16.54, 16.23. ESI-HRMS (m/z): calcd for $C_{37}H_{64}NO_5^+$ $[M + H]^+$: 634.4677, found: 634.4665.

2.4. Cytotoxic (MTT assay)

Hep3B cells were cultured in a 96-well plate at a density of 5×10^4/well, in 200 μL medium, and cultured for 12 h to allow them to adhere. Then, 20(*R*)-panaxotriol and its derivatives were processed according to a concentration gradient (final concentrations of 0.3, 1, 3, 10, and 30 μM), each concentration was repeated three times, and the cells were cultured for 24 h. The incubation was continued for 4 h after the addition of the thiazole blue reagent in the dark. After removing the thiazole blue reagent, 150 μL of dimethyl sulfoxide was added for coloring and dissolved by shaking for 10 min. The absorbance (optical density, OD) was measured at a wavelength of 492 nm on a microplate reader, and the data were analyzed.

2.5. Luciferase reporter assay

When the Hep3B cells reached 60%–80% confluence, they were used for plasmid transfection. The medium was changed, Lipofectamine 2000 was used to transfect the cells with pGL-HRE-Luc plasmid, and the cells were cultured for 24 h. After digesting the cells with trypsin, they were seeded into a 96-well plate (5×10^4/well, 200 μL) and incubated for 24 h to allow adherence. The cells were treated with a concentration gradient of 20(*R*)-panaxotriol and its derivatives (final concentrations of 0.3, 1, 3, 10, and 30 μM). Three replicate wells were prepared for each concentration, and cells were cultured for 12–16 h. The medium was aspirated, 80 μL of cell lysate was added to each well (5 × cell lysate was diluted with 3:1 distilled water), and the plate was shaken on a shaker for 1 h to fully lyse the cells. Then, 30 μL of lysed cells per well was added to the white plate. The OD was measured using Luminoskan, and the data were analyzed.

2.6. Molecular docking

A molecular docking study was performed to investigate the binding mode of the compound **A11** to HIF-1α protein using the Discovery Studio 2017/CDOCKER protocol (Accelrys, San Diego, USA), according to a previously described method [46]. HIF-1α structure was obtained from the Protein Data Bank (https://www.rcsb.org, PDB ID: 4ZPR). Compound **A11** was treated with the ligand preparation and minimization models in Discovery Studio 2017 to investigate the binding patterns of compound **A11** and HIF-1α LBD.

2.7. Western blotting

Cell extracts were analyzed using western blotting [47,48]. HeLa cells were incubated with 3, 10, and 30 μM of compound **A11** for 12 h. Cells were lyse in an ice-cold lysis buffer to obtain the nuclear extract protein. A bicinchoninic acid protein quantitative detection kit was used to quantify the protein at 570 nm. Sodium dodecyl sulfate-polyacrylamide gel was used to separate 30 μg of nuclear extract protein per lane, and then the protein bands were transferred to polyvinylidene fluoride membranes (Hybond-P). Membranes were blocked with 5% nonfat milk and then incubated with the corresponding antibodies at 4 °C overnight, followed by incubation with secondary antibodies for 2 h, and detection with a high-efficiency chemiluminescence kit.

2.8. Immunofluorescence staining

HeLa cells were cultured for 24 h on a 24-well plate (1×10^4/well) to facilitate adherence, and treated with the derivative **A11** (final concentration 30 μM) for 12h. The cells were rinsed with phosphate-buffered saline (PBS), fixed with 4% paraformaldehyde at room temperature for half an hour, and then permeabilized in 0.2% Triton X-100. They were blocked in 5% bovine serum albumin for half an hour, incubated with the HIF-1α antibody at 4 °C overnight, followed by incubation with a secondary antibody at room temperature for half an hour. They were finally stained with 4′, 6-diamidino-2-phenylindole for half an hour, and observed under a fluorescence microscope. Blue color represent the nucleus and green represents the HIF-1α protein. The green and blue-colored images were merged using NIS-Elements software.

2.9. Colony formation assay

HeLa cells were incubated for 12 h in a 6-well plate (1×10^3/well). After changing to a new medium, the cells were treated with the derivative **A11** (final concentrations of 3, 10, and 30 μM) and incubated for 10 days until the colonies were clearly visible. Next, the cells were rinsed in 1 mL of PBS, fixed in 700 μL of 10% formaldehyde, stained in 700 μL of 1% crystal violet, washed with 1 mL of PBS three times, and naturally air-dried.

2.10. 5-ethynyl-2′-deoxyuridine (EdU) labeling and immunofluorescence

HeLa cells were incubated for 24 h in a 96-well plate (5×10^4/well). After treatment with the derivative **A11** (final concentrations of 3, 10, and 30 μM), the cells were incubated for 12 h, followed by incubation with EdU (RiboBio, Guangzhou, China) for 1 h. The cells were then fixed with 4% paraformaldehyde for 30 min, treated with 0.5% Triton X-100 for 10 min, and washed in PBS. They were then incubated in a 1 × Apollo® reaction cocktail for half an hour and stained with Hoechst 33,342. Finally, the stained cells were visualized using an Olympus IX83 inverted fluorescence microscope.

2.11. Apoptosis assay

Apoptosis was analyzed using flow cytometry, as previously described [49]. Apoptosis was detected using the Annexin V-FITC Apoptosis Detection Kit (BD Biosciences). Briefly, the HeLa cells were cultured for 24 h in a 6-well plate (5×10^5/well) and incubated for 24 h after treatment with derivative **A11** (final concentrations of 3, 10, and 30 μM). Then, the cells were collected, washed

twice with PBS, and mixed with the binding buffer (10 mM 4-(2-hydroxyethyl)-1-piperazineëthanesulfonic acid (HEPES), pH 7.4, 140 mM NaCl, 2.5 mM $CaCl_2$). The cells were then stained with Annexin V-FITC and 2 μg/mL propidium iodide in a dark environment at 37 °C for 15 min. Analysis was performed by flow cytometry after the addition of 400 μL binding buffer to the samples. Cell Quest software (Becton-Dickinson, Franklin Lakes, NJ, USA) was used to analyze the data.

2.12. Cell migration assay

Scratch experiments were performed to detect the migration of HeLa cells. The cells were inoculated in a 24-well plate (1×10^5/well) and incubated for 24 h tofacilitate adherence. A sterile pipette tip was used to make vertical scratches in each hole, and the plates were washed thrice with PBS to remove the scratched cells. The medium was then replaced with a serum-free medium. After treatment with the derivative **A11** (final concentrations of 3, 10, and 30 μM), the cells were incubated for 12 h. Images were taken with a fluorescence microscope to observe the degree of migration of the cells to the scratched area.

2.13. Transwell assay

The invasion assay was performed using a Transwell chamber (Costar, MA, USA). The Transwell membrane was coated with Matrigel (BD Biocoat, Bedford, MA, USA) for the invasion assay and the cells pretreated with or without **A11** (3, 10, and 30 μM) in serum-free DMEM were added to the upper compartment of the chamber. The lower compartment contained DMEM supplemented with 10% FBS. After 24 h of invasion at 37 °C, the cells migrated to the bottom chamber were fixed with 4% paraformaldehyde and stained with 0.1% crystal violet. Then, the cells were photographed under a microscope.

2.14. In vivo antitumor activity

Male athymic Nu/Nu nude mice (4–5 weeks of age, 24 ± 2 g; Vital River Laboratory Animal, Beijing, China) were reared under septic conditions as per the Guidelines for the Care and Use of Laboratory Animals (NIH Publication No. 85-23, revised 1996). Normal saline (200 μL) was injected subcutaneously into the mice with HeLa cells. Two weeks later, the mice were randomly divided into five groups (n = 4), 50 mg/kg **A11**, 30 mg/kg **A11**, 30 mg/kg 20(*R*)-panaxotriol, 30 mg/kg 5-fluorouracil, and a negative control group. An intraperitoneal injection was administered every two days, and the body weights and tumor volumes of mice were simultaneously measured for 20 days. On the 21st day, the mice were sacrificed, and the tumors were excised and weighed. The following standard formula was used to calculate the tumor volume (mm^3): (length × (width)^2)/2. Ratio of inhibition of tumor (%) = (1 - average tumor weight of treated group/average tumor weight of control group) × 100%.

2.15. Statistical analysis

All data are presented as the mean ± standard deviation (SD), and all experiments were independently performed in triplicate. A comparison of the results was performed using one-way analysis of variance and Tukey's multiple comparison tests (GraphPad Software, Inc. San Diego, CA, USA). Statistically significant differences between the groups were defined as $p < 0.05$.

3. Results and discussion

3.1. Chemistry

Fig. 1**A** illustrates the synthesis of intermediate. Compounds **1a-1c** were obtained through diazotization and azidation of different anilines [50]. After that, the click process between propionic acid and intermediates **1a-1c** yielded intermediates **2a-2c** [51,52]. Cinnamic acid intermediates **3a-3c** were synthesized by the Knoevenagel condensation reaction of various benzaldehydes and malonic acid [53].

Fig. 1**B** shows the general process for the synthesis of target 20(*R*)-panaxotriol analogs **A1-A15**, **B1-12**, and **C1-C12**. Derivatives **A1-A3**, **B1-B3**, and **C1-C3** are formed by the condensation of 20(*R*)-panaxotriol with isocyanate under alkaline conditions, and the yield ranged from 8% to 64%. In addition, 20(*R*)-panaxotriol undergoes a condensation reaction with various carboxylic acids to generate derivatives **A4-A12**, **B4-B12**, and **C4-C12**, with DMAP and EDC used as condensing agents, and yields ranging from 5% to 58%. Derivatives **A13-A15** were derived from derivatives **A10-A12** after removing t-butyloxy carbonyl, with yields ranging from 75% to 97%. The structures of the desired compounds were characterized by ^{1}H-NMR and ^{13}C-NMR spectroscopy and high-resolution mass spectrometry (Supporting Materials).

3.2. Biological evaluation

3.2.1. In vitro HIF-1α inhibitory activity and SAR study

MTT assay determined the cytotoxicity of 20(*R*)-panaxotriol and its derivatives in Hep3B cells. The results in **Figure 2A** show that, except for **A13** (IC_{50} = 6.99 μM), all other compounds exhibited no cytotoxicity (IC_{50} > 30 μM). To detect the effect of 20(*R*)-panaxotriol and its derivatives on the transcriptional activity of HIF-1, a luciferase reporter gene experiment was performed on human liver cancer cells Hep3B (Fig. 2A), with 20(*R*)-panaxotriol as a positive control. The great majority of the derivatives had inhibitory effects on HIF-1α and were stronger than the positive control 20(*R*)-panaxotriol. Among them, the compound **A11** with t-butyloxycarbonyl-glycine was the most effective derivative, and its IC_{50} for inhibiting HIF-1α transcription activity in the Hep3B cell line was <0.3 μM. Its efficacy was over 100 times higher than that of 20(*R*)-panaxotriol. The derivatives **C1-C12** inhibited transcription of HIF-1α weaker than those of derivatives **A1-A12** and **B1-B12**, especially aminotriazoles and cinnamic acids (derivatives **C4-C9**: IC_{50} > 30 μM), indicating that the double-modified derivatives at the C-3 and C-6 positions of 20(*R*)-panaxotriol have weaker activity than the C-3 or C-6 single-modified derivatives. Among 20(*R*)-panaxotriol isocyanate derivatives, the C-3 monosubstituted derivatives had the best activity with a benzene ring **A2** (IC_{50} = 1.58 μM), and the C-6 monosubstituted derivatives with cycloalkyl **B3** had the best activity (IC_{50} = 1.08 μM), the activity of the cycloalkyl group in the C-3 and C-6 disubstituted derivatives **C3** was the highest (IC_{50} = 14.85 μM). This shows that the aromatic ring and cycloalkyl are equally important in 20(*R*)-panaxotriol isocyanate derivatives. For the 20(*R*)-panaxotriol derivatives with phenyl-1,2,3 triazole mono-substituted at the C-3 position, the electron donating group showed better effects than the electron withdrawing group (*p*-OCH_3 > *p*-H > *p*-Cl) (IC_{50} are 0.33 μM, 0.43 μM, and >30 μM, respectively). Unfortunately, no clear structure-activity relationship has been found in cinnamic acid-substituted 20(*R*)-panaxotriol derivatives. It can be seen from the derivatives **A10-A15** that the influence of the protection of the tert-butoxycarbonyl group in amino acids on the inhibition of HIF-1α transcription activity is not obvious (Fig. 2B). These findings indicate that 20(*R*)-panaxotriol

A

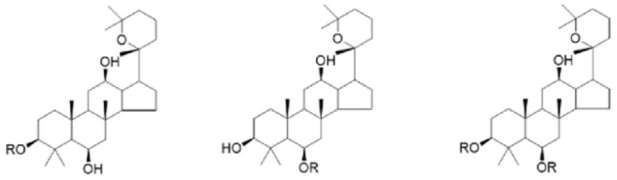

R	R_1	Compd	IC_{50} (μM) HRE[a]	IC_{50} (μM) Cytotoxic activity[b]	Compd	IC_{50} (μM) HRE[a]	IC_{50} (μM) Cytotoxic activity[b]	Compd	IC_{50} (μM) HRE[a]	IC_{50} (μM) Cytotoxic activity[b]
	$-CH_2C_6H_5$	A1	11.22 ± 0.08	> 30	B1	3.81 ± 0.15	> 30	C1	> 30	> 30
	$-C_6H_5$	A2	1.58 ± 0.07	> 30	B2	5.47 ± 0.11	> 30	C2	15.86 ± 0.12	> 30
	C_6H_{11}	A3	4.09 ± 0.12	> 30	B3	1.08 ± 0.12	> 30	C3	14.85 ± 0.11	> 30
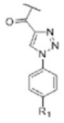	-H	A4	0.43 ± 0.06	> 30	B4	> 30	> 30	C4	> 30	> 30
	$-OCH_3$	A5	0.33 ± 0.10	> 30	B5	> 30	> 30	C5	> 30	> 30
	-Cl	A6	> 30	> 30	B6	> 30	> 30	C6	> 30	> 30
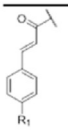	-H	A7	> 30	> 30	B7	2.39 ± 0.12	> 30	C7	> 30	> 30
	$-OCH_3$	A8	1.47 ± 0.08	> 30	B8	15.64 ± 0.09	> 30	C8	> 30	> 30
	-Cl	A9	6.07 ± 0.07	> 30	B9	6.59 ± 0.11	> 30	C9	> 30	> 30
	$3\text{-}CH_2$-indole	A10	4.89 ± 0.12	> 30	B10	1.25 ± 0.16	> 30	C10	11.36 ± 0.16	> 30
	-H	A11	**< 0.3**	> 30	B11	2.04 ± 0.23	> 30	C11	2.71 ± 0.11	> 30
	$-CH(CH_3)_2$	A12	1.95 ± 0.15	> 30	B12	0.54 ± 0.09	> 30	C12	> 30	> 30
	$3\text{-}CH_2$-indole	A13	2.11 ± 0.28	6.99 ± 0.32						
	-H	A14	2.81 ± 0.09	> 30						
	$-CH(CH_3)_2$	A15	1.51 ± 0.15	> 30						
	20(*R*)- panaxotriol		> 30	> 30						

B

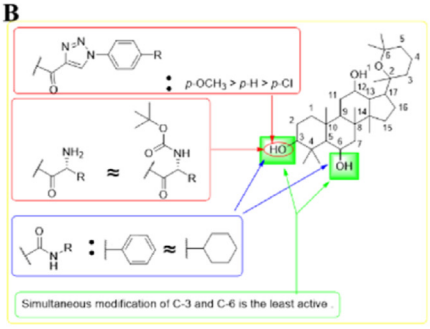

C

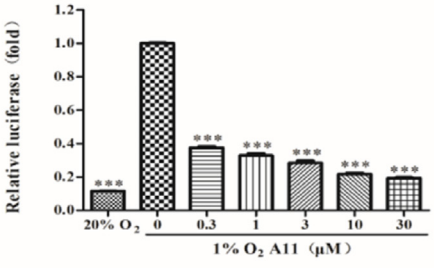

D

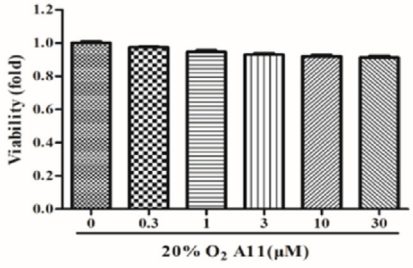

Fig. 2. (A) In vitro inhibition of HIF-1α transcriptional activity in cell-based HRE reporter assay under hypoxia conditions and cytotoxic activity. [a] The inhibitory effects of all the derivatives on HIF-1α transcriptional activity were tested by HRE luciferase reporter assay after 24 h treatment of Hep3B cells under hypoxic conditions. Values were shown as mean ± SD, n = 3. [b] The cytotoxic activity was evaluated by MTT assay after 24 h treatment of compounds under normoxic conditions. Values were shown as mean ± SD, n = 3. (**B**) The structures of 39 derivatives of 20(*R*)-panaxotriol for their structure-activity-relationships. (**C**) Effect of compound **A11** on HRE-mediated reporter gene expression. Hep3B cells were transiently co-transfected with a pGL3-HRE-Luciferase and pRL-CMV vectors. Following 24 h incubation, the cells were incubated under hypoxia in the absence or presence of the indicated concentrations of compound **A11**. Luciferase activities were determined as described in "Materials and Methods". Data are represented as the mean ± standard deviation of three independent experiments. *$p < 0.05$, **$p < 0.01$, ***$p < 0.001$, significant with respect to the hypoxia control. (**D**) Hep3B cells were treated with the indicated concentrations of compound **A11**. After 24 h incubation, cell viability was determined by MTT assays.

derivatives effectively reduced the level of HIF-1α without significant cytotoxicity in Hep3B cells.

Further activity analysis was conducted on derivative **A11** with the best HIF-1α inhibitory activity. The results in Fig. 2C and Fig. 2D show that, compared with 20% oxygen situation, under 1% oxygen situation, the transcription activity of HIF-1α was significantly increased ($p < 0.001$). After adding 0.3 μM of derivative **A11**, the transcription activity of HIF-1α was reduced. As the concentration of the derivative **A11** drug increased, the transcriptional activation of HIF-1α decreased. The results indicated that derivative **A11** dose-dependent inhibited the transcriptional activity of HIF-1α (Fig. 2C). Derivative **A11** at concentrations as high as 30 μM had no adverse effects on cell viability (Fig. 2D).

3.2.2. Compound *A11* inhibits HIF-1α protein expression in HeLa cells

To explore the interaction between compound **A11** and HIF-1α, we investigated its binding mode through a molecular docking study. As shown in Fig. 3A, the central structure of compound **A11** was considered to form conventional hydrogen bond interactions with surrounding residues (Cys351, Gln359, and His286), and the *t*-butoxycarbonyl part of compound **A11** was considered to form a mixed pi/alkyl hydrophobic interaction with the surrounding residues (Arg156, Pro154 and Met354). Moreover, the nitrogen atom of the amino acids of compound **A11** formed a hydrogen bond with Ser355. We also found that the compound **A11** showed good binding interactions with the related protein (4ZPR) in the binding pocket. Western blotting determined the effect of compound **A11** on the expression of HIF-1α protein in HeLa cells. As shown in Fig. 3B, under normoxic conditions, HIF-1α was not expressed. Under 1% O_2 conditions, HIF-1α was shown to accumulate in large amounts. The addition of different concentrations of **A11** dose-dependently reduced the HIF-1α protein content in HeLa cells. However, **A11** had almost no influence on the expression level of HIF-1β. Next, we performed an immunofluorescence experiment to determine whether compound **A11** inhibited the increase of HIF-1α in the nucleus of HeLa cells. The results in Fig. 3C show that, in the nucleus, the HIF-1α protein was not expressed under normoxic conditions. Under 1% O_2 conditions, in the nucleus, the HIF-1α protein was largely amassed; however, after adding 30 μM of compound **A11**, HIF-1α expression in the nucleus was not detected. These results indicate that compound **A11** inhibited nuclear accumulation of HIF-1α.

HIF-1α is known to regulate the expression of VEGF, a crucial growth factor involved in tumor cell proliferation, angiogenesis, invasion, and metastasis [9,54]. Therefore, in this study, we tested the effect of **A11** on VEGF protein expression by western blotting, We found that hypoxic conditions significantly increased the expression levels of VEGF, while treatment with **A11** resulted in a dose-dependent decrease in its levels (Fig. 3D), and the effective concentrations were comparable to those inhibiting HIF-1α protein expression.

3.2.3. Compound *A11* inhibits HeLa cell proliferation and promotes apoptosis

Malignant tumor cells can grow without restriction. Colony forming test can determine the size of cell colony formation [55]; thus, the colony formation test can evaluate the inhibitory ability of **A11** on cell multiplication more directly. The results in Fig. 4A show that, compound **A11** apparently inhibited the colony formation of cells, and the inhibitory effect became more obvious when the concentration was increased. The EdU experiment yielded similar results. As shown in Fig. 4B, compared with the control group, compound **A11** concentration-dependently suppressed the number of EdU-positive cells. In addition, we wanted to confirm whether compound **A11** could induce cell apoptosis in addition to inhibiting cell multiplication. Therefore, Annexin V-FITC/PI double staining was performed. As shown in Fig. 4C, compared with the control group, incubation with compound **A11** (3, 10, and 30 μM) resulted in a concentration-dependent increase in the percentage of total apoptotic (early and late) cells (5.2%, 14.0%, and 24.2%, respectively). These results indicated that compound **A11** could effectively induce cell apoptosis. To further understand the anti-apoptotic effects, western blotting analysis was used to determine the expression levels of cleaved-caspase 3, Bcl-2, and Bax proteins *in vivo*. As shown in Fig. 4D, the expression levels of Bax were increased in the compound **A11**-treated HeLa cells compared to those in the control group, whereas the levels of Bcl-2 were decreased after treatment with compound **A11**. Therefore, the ratio of Bax/Bcl-2 increased in a dose-dependent manner. In addition, it was observed that with the treatment of compound **A11** (0, 3, 10, and 30 μM), the expression levels of cleaved caspase-3 in HeLa cells significantly increased in a concentration-dependent manner. Taken together, these data further confirmed that compound **A11** could induce apoptosis in HeLa cells.

3.2.4. Compound *A11* inhibits HeLa cell migration and invasion

Because HIF-1α is a key regulator of tumor invasion [56,57], we performed cell scratch assay and transwell assay to study the effect of compound **A11** on HeLa cell motility. The results showed that the migration of HeLa cells in the cells treated with compound **A11** decreased compared with the control group, and the degree of reduction in the migration of HeLa cells increased as the concentration of compound **A11** increased. Treatment with compound **A11** significantly reduced the number of tumor cells that crossed the transwell chamber compared to the control. Moreover, the invasion and migration of HeLa cells decreased to a greater extent at an increased dose of **A11**, suggesting that **A11** inhibited the invasion and migration of HeLa cells in a concentration-dependent manner (Fig. 5A and Fig. 5B). Next, the effect of **A11** on the expression of the invasion and migration-associated protein, MMP-9, was investigated. Western blotting experiments showed that treatment with **A11** (10 μM) significantly reduced the expression levels of MMP-9 (Fig. 5C), further confirming that **A11** plays an inhibitory role in the migration and invasion of HeLa cells.

3.2.5. In vivo antitumor activity of compound *A11*

Antitumor activity of compound **A11** was remarkable *in vitro*, prompting us to verify its antitumor effect *in vivo*. The measured nude mouse body weight and nude mouse tumor volume results are shown in Fig. 6A and 6B. In the control group, the average tumor volume was obviously larger than that in the 20(*R*)-panaxotriol, **A11**, and 5-fluorouracil treatment groups. **A11** significantly inhibit tumor volume ($p < 0.001$). But, the mice in the control group and other groups had very little difference in body weight, and this difference was not statistically significant. This indicates that the treatment could not produce toxicity *in vivo*. After administration of the treatment to nude mice, the nude mice were died by spinal dislocation, and the solid tumor was removed and photographed. The experimental results are shown in Fig. 6C. It can be seen more clearly from the figure that compared with the control group, the **A11** group was associated with inhibition of cancer cell growth. The tumor growth inhibition rates in mice treated with 30 mg/kg 20(*R*)-panaxotriol, 30 mg/kg **A11**, 50 mg/kg **A11**, and 30 mg/kg 5-fluorouracil were 40.15%, 70.33%, 76.21%, and 61.89%, respectively (Fig. 6D). According to the above pharmacological data, *in vivo*, the antitumor ability of derivative **A11** was remarkably stronger than that of 20(*R*)-panaxotriol ($p < 0.01$). In addition, the antitumor activity of **A11** increased as its concentration increased.

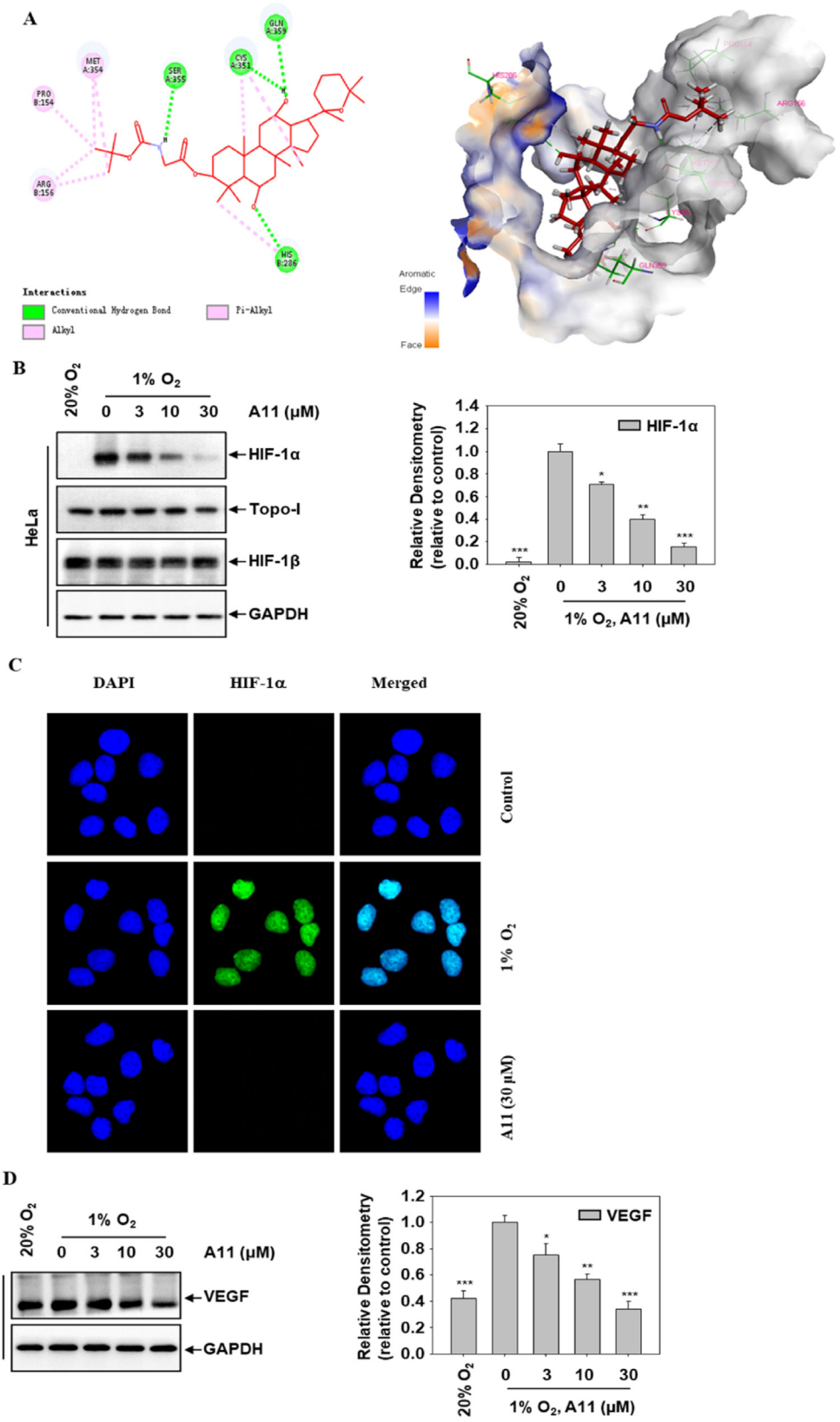

Fig. 3. (**A**) compound **A11** was docked into the binding site of HIF-1α (2D binding mode and 3D binding mode) (PDB ID: 4ZPR). The ligand is shown in red. (**B**) HeLa cells were incubated under normoxia or hypoxia for 12 h in the absence or presence of indicated concentrations of **A11**. Whole-cell lysates for HIF-1β and nuclear extract for HIF-1α were analyzed using western blotting. Data are respresented as the mean ± standard deviation of three independent experiments. *$p < 0.05$, **$p < 0.01$, ***$p < 0.001$, significant with respect to the hypoxia control. (**C**) HeLa cells were incubated with or without **A11** (30 μM) under normoxia or hypoxia for 12 h and then analyzed for the intracellular distribution of HIF-1α by immunofluorescence assay (magnification, 400×). (D) HeLa cells were incubated under normoxia or hypoxia for 12 h in the absence or presence of indicated concentrations of **A11**. VEGF were analyzed using western blotting. Data are respresented as the mean ± standard deviation of three independent experiments. *p < 0.05, **p < 0.01, ***p < 0.001, significant with respect to the hypoxia control.

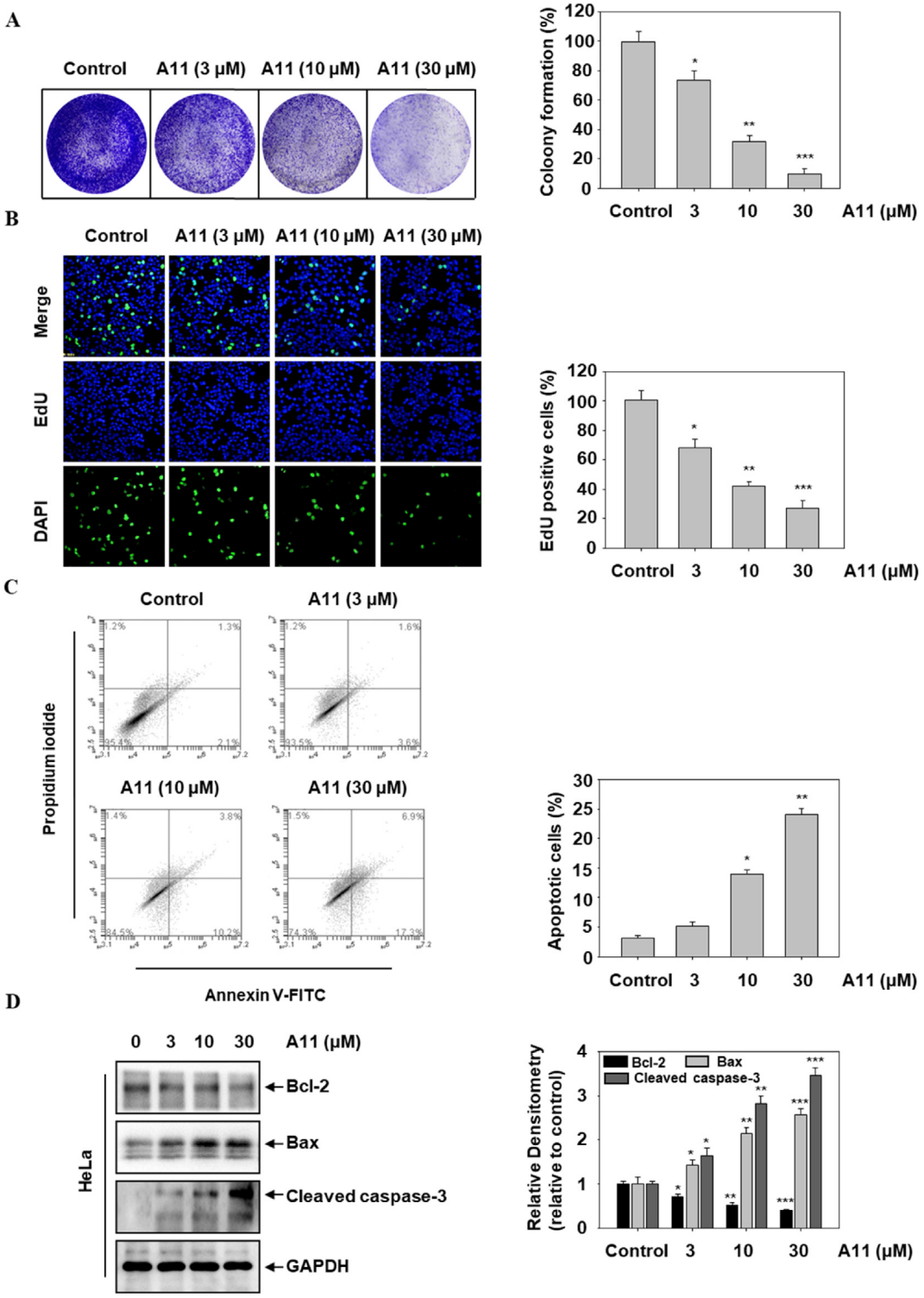

Fig. 4. HeLa cells were incubated under hypoxic for 12 h in the absence or presence of **A11** (3, 10 and 30 μM). Cells proliferation was measured by colony formation assay (**A**) EdU assay (**B**) and Apoptosis assay (**C**). (**D**) HeLa cells were treated with or without **A11** (3, 10 and 30 μM) for 12h. Whole cell extracts were analyzed by Western blot analysis using Bax, Bcl-2 and Cleaved Caspase-3. Data represented as mean ± standard deviation of three independent experiments. *p < 0.05, **p < 0.01, ***p < 0.001, significantly different when compared with control group.

4. Conclusion

For the study, 39 new C-3 and C-6 derivatives of 20(*R*)-panaxotriol were designed and synthesized, and their HIF-1α transcription inhibitory activities were studied. Most of the derivatives showed strong HIF-1α transcription inhibitory activity. Among them, the derivative **A11** with *t*-butyloxycarbonyl-glycine showed the strongest HIF-1α transcription inhibitory activity, and its IC_{50} for inhibiting HIF-1α transcription activity in the Hep3B cell line was <0.3 μM. Its efficacy was shown to be over 100 times higher

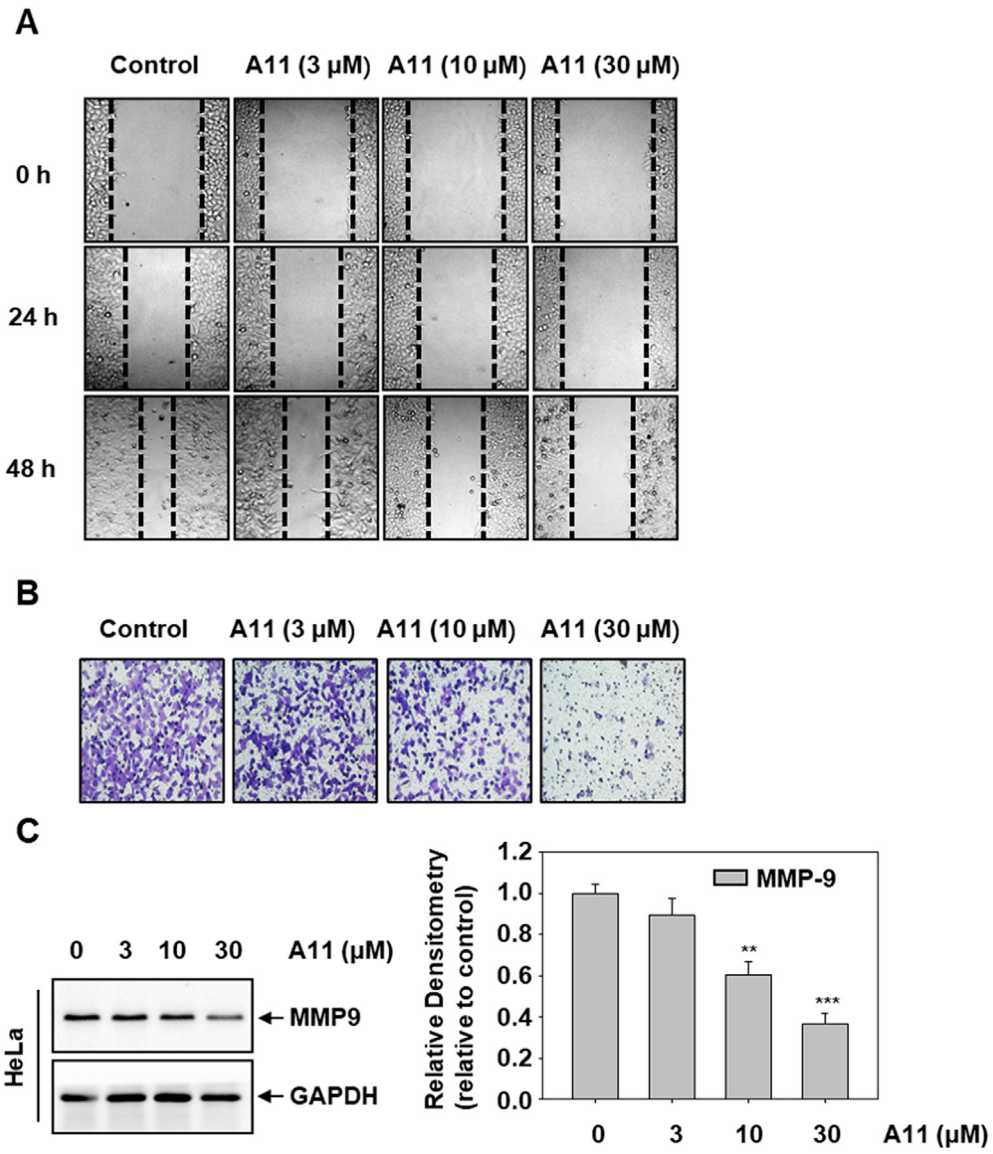

Fig. 5. (A) HeLa cells were incubated under hypoxic for 12 h in the absence or presence of **A11** (3, 10 and 30 μM). HeLa cell migrations were photographed at identical locations and cell migration was analyzed by comparing final gap width to initial gap width. Original magnification, 200×. (B) HeLa cells were seeded into the matrigel coated transwell chamber and exposed to **A11** (3, 10 and 30 μM) for 12 h to evaluated the invasion activity. The cells at the lower side of the membrane were then stained using Crystal Violet. Original magnification, 200×. (C) HeLa cell was treated with or without **A11** (3, 10 and 30 μM) for 12h. Whole cell extracts were analyzed by Western blot analysis using MMP-9. Data represented as mean ± standard deviation of three independent experiments. *p < 0.05, **p < 0.01, ***p < 0.001, significantly different when compared with control group.

than that of 20(*R*)-panaxotriol. The results of molecular docking highlight that glycine with *t*-butyloxycarbonyl on C-3 of 20(*R*)-panaxotriol may be important for good HIF-1α inhibition. In addition, derivative **A11** dose-dependently inhibited the transcriptional ability of HIF-1α, dose-dependently inhibited HIF-1α protein content in HeLa tumor cells, and inhibited the nuclear accumulation of HIF-1α. **A11** was also observed to dose-dependently inhibit HeLa cell proliferation and promote apoptosis, as well as inhibit migration of HeLa cells. Furthermore, in the HeLa cervical cancer xenograft model, compound **A11** significantly inhibited tumor volume by 76.21% (50 mg/kg) and 70.33% (30 mg/kg) (ip). It was better than 20(*R*)-panaxotriol (40.15%) and 5-fluorouracil (61.89%). In short, derivative **A11** shows excellent antitumor activity *in vivo* and *in vitro*, and may be used as an effective antitumor agent in the future after more in-depth research. So far, only a few types of 20(*R*)-panaxotriol derivatives with amino acids have been synthesized, and there may be certain compounds that have better activity than **A11**, Therefore, more follow-up studies are needed to explore and analyze such compounds in the future.

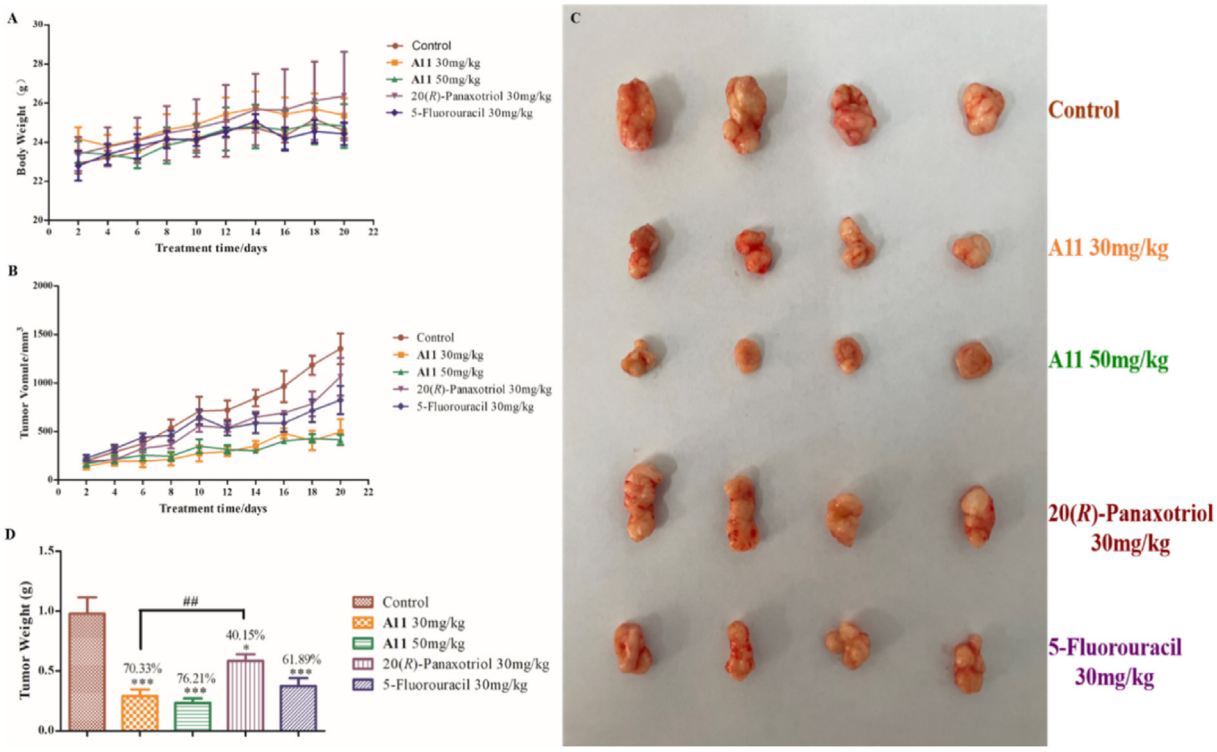

Fig. 6. Compound **A11** inhibits cervical cancer xenograft growth *in vivo*. (**A**) The mice were randomly divided into five groups with 4 mice in each group and treated intraperitoneally with control, **A11** (30 mg/kg), **A11** (50 mg/kg), 20(*R*)-panaxotriol (30 mg/kg) and 5-fluorouracil (30 mg/kg) every two days for 20 days and the figure showed the average measured body weight. (**B**) Tumour volumes of mice before dissection. (**C**) The resulting tumors were excised from the animals after treatment. (**D**) Histograms display the changes of tumour weight, *$p < 0.05$, **$p < 0.01$, and ***$p < 0.001$ compared with control group; ##$p < 0.01$ compared with 20(*R*)-panaxotriol group.

Declaration of competing interest

The authors have no conflicts of interest to report.

Acknowledgements

This work was supported by the National Natural Science Foundation of China, China (No.81960626, 82060628), Doctoral Research Startup Fundation of Yanbian University (No. 602020087), Higher Education Discipline Innovation Project, China (111 Project, D18012), and Jilin Provincial Department of Education Science and Technology Research Project, China (NO. JJKH20220559KJ).

Appendix A. Supplementary data

Supplementary data to this article can be found online at https://doi.org/10.1016/j.jgr.2022.03.001.

References

[1] Jemal A, Bray F, Center MM, Ferlay J, Ward E, Forman D. Global cancer statistics. CA Cancer J Clin 2011;61:69–90.
[2] Ferlay J, Soerjomataram I, Dikshit R, Eser S, Mathers C, Rebelo M, Parkin DM, Forman D, Bray F. Cancer incidence and mortality worldwide: sources, methods and major patterns in GLOBOCAN 2012. Int J Cancer 2015;136:E359–86.
[3] Hait WN. Anticancer drug development: the grand challenges. Nat Rev Drug Discov 2010;9:253–4.
[4] Arbyn M, Weiderpass E, Bruni L, de Sanjosé S, Saraiya M, Ferlay J, Bray F. Estimates of incidence and mortality of cervical cancer in 2018: a worldwide analysis. Lancet Global Health 2020;8:e191–203.
[5] Powis G, Kirkpatrick L. Hypoxia inducible factor-1alpha as a cancer drug target. Mol Cancer Ther 2004;3:647–54.
[6] Vaupel Peter, Mayer Arnulf, Höckel M. Tumor hypoxia and malignant progression. Methods Enzymol 2004;381:335–54.
[7] Semenza GL. Defining the role of hypoxia-inducible factor 1 in cancer biology and therapeutics. Oncogene 2010;29:625–34.
[8] Ke Q, Costa M. Hypoxia-inducible factor-1 (HIF-1). Mol Pharmacol 2006;70:1469–80.
[9] Semenza GL. Targeting HIF-1 for cancer therapy. Nat Rev Cancer 2003;3:721–32.
[10] Pientka FK, Hu J, Schindler SG, Brix B, Thiel A, Johren O, Fandrey J, Berchner-Pfannschmidt U, Depping R. Oxygen sensing by the prolyl-4-hydroxylase PHD2 within the nuclear compartment and the influence of compartmentalisation on HIF-1 signalling. J Cell Sci 2012;25:5168–76.
[11] Li MY, Mi C, Wang KS, Wang Z, Zuo HX, Piao LX, Xu GH, Li X, Ma J, Jin X. Shikonin suppresses proliferation and induces cell cycle arrest through the inhibition of hypoxia-inducible factor-1alpha signaling. Chem Biol Interact 2017;274:58–67.
[12] Lu Y, Li Y, Wang Z, Xie S, Wang Q, Lei X, Ruan Y, Li J. Downregulation of RGMA by HIF-1A/miR-210-3p axis promotes cell proliferation in oral squamous cell carcinoma. Biochem Pharmacol 2019;112:108608.
[13] Yao J, Man S, Dong H, Yang L, Ma L, Gao W. Combinatorial treatment of Rhizoma Paridis saponins and sorafenib overcomes the intolerance of sorafenib. J Steroid Biochem Mol Biol 2018;183:159–66.
[14] Zhu X, Shen H, Yin X, Yang M, Wei H, Chen Q, Feng F, Liu Y, Xu W, Li Y. Macrophages derived exosomes deliver miR-223 to epithelial ovarian cancer cells to elicit a chemoresistant phenotype. J Exp Clin Cancer Res 2019;38:81.
[15] Choi KJ, Baik IH, Ye SK, Lee YH. Molecular targeted therapy for hepatocellular carcinoma: present status and future directions. Biol Pharm Bull 2015;38:986–91.
[16] Wu J, Joseph SO, Muggia FM. Targeted therapy: its status and promise in selected solid tumors part I: areas of major impact. Oncology (Williston Park) 2012;26:936–43.
[17] Hodges TW, Hossain CF, Kim YP, Zhou YD, Nagle DG. Molecular-targeted antitumor agents: the Saururus cernuus dineolignans manassantin B and 4-O-demethylmanassantin B are potent inhibitors of hypoxia-activated HIF-1. J Nat Prod 2004;67:767–71.
[18] Yuan SM. Potential cardioprotective effects of Ginseng preparations. Pak J Pharm Sci 2015;28:963–8.
[19] Attele AS, Wu JA, Yuan C-S. Ginseng pharmacology. Biochem Pharmacol 1999;58:1685–93.
[20] Kim JH. Pharmacological and medical applications of Panax ginseng and ginsenosides: a review for use in cardiovascular diseases. J Ginseng Res 2018;42:264–9.
[21] Shibata S. Chemistry and cancer preventing activities of ginseng saponins and some related triterpenoid compounds. J Kor Med Sci 2001;16(Suppl):S28–37.

[22] Park JD, Rhee DK, Lee YH. Biological activities and chemistry of saponins from Panax ginseng C. A. Meyer. Phytochem Rev 2005;4:159–75.
[23] Wei Y, Ma C-M, Hattori M. Anti-HIV protease triterpenoids from the acid hydrolysate of Panax ginseng. Phytochem Lett 2009;2:63–6.
[24] Yu R, Zhang Y, Xu ZQ, Wang JJ, Chen BC, Jin H. Potential antitumor effects of panaxatriol against DU-15 human prostate cancer cells is mediated via mitochondrial mediated apoptosis, inhibition of cell migration and sub-G1 cell cycle arrest. J Buon 2018;23:200–4.
[25] Li JL, Ding P, Jiang B, Yang M, Ren J, Song Y, Chen G. Biotransformation of 20(R)-panaxatriol by the fungus Aspergillus flavus link AS 3.3950. Nat Prod Res 2019;33:1393–8.
[26] Sheng C, Zhang W. New lead structures in antifungal drug discovery. Curr Med Chem 2011;18:733–66.
[27] Neu HC, Fu KP. Cefatrizine activity compared with that of other cephalosporins. Antimicrob Agents Chemother 1979;15:209–12.
[28] Soltis MJ, Yeh HJ, Cole KA, Whittaker N, Wersto RP, Kohn EC. Identification and characterization of human metabolites of CAI [5-amino-1-1(4'-chlorobenzoyl-3,5-dichlorobenzyl)-1,2,3-triazole- 4-carboxamide). Drug Metab Dispos 1996;24:799–806.
[29] Higashitani F, Hyodo A, Ishida N, Inoue M, Mitsuhashi S. Inhibition of beta-lactamases by tazobactam and in-vitro antibacterial activity of tazobactam combined with piperacillin. J Antimicrob Chemother 1990;25:567–74.
[30] Zhang G-R, Ren Y, Yin XM, Quan ZS. Synthesis and evaluation of the anticonvulsant activities of new 5-substitued-[1,2,4]triazolo[4,3-a]quinoxalin-4(5H)-one derivatives. Lett Drug Des Discov 2018;15:406–13.
[31] Liu X-J, Zhang H-J, Quan Z-S. Synthesis and evaluation of the anticonvulsant activities of 2,3-dihydrophthalazine-1,4-dione derivatives. Med Chem Res 2017;26:1935–46.
[32] Ren Y, Shen QK, Ding MM, Yin XM, Quan ZS. Synthesis and anticonvulsant activities of 4-Alkoxyl-[1,2,4]Triazolo[4,3-a]Quinoxaline derivatives. Lat Am J Pharm 2016;35:2169–75.
[33] Liu CF, Zhang HJ, Quan ZS. Synthesis and anticonvulsant activity of novel 3-(2-(4H-1,2,4-triazol-4-yl)ethyl)-1-alkyl-1H-indole derivatives. Lett Drug Des Discov 2016;13:833–9.
[34] Zhang H-J, Wang S-B, Wen X, Li J-Z, Quan Z-S. Design, synthesis, and evaluation of the anticonvulsant and antidepressant activities of pyrido[2,3-d]pyrimidine derivatives. Med Chem Res 2016;25:1287–98.
[35] Pang L, Liu CY, Gong GH, Quan ZS. Synthesis, in vitro and in vivo biological evaluation of novel lappaconitine derivatives as potential anti-inflammatory agents. Acta Pharm Sin B 2020;10:628–45.
[36] Pan F-J, Wang S-B, Liu D-C, Gong G-H, Quan Z-S. Synthesis of 4-Phenylthieno [2,3-e][1,2,4]triazolo[4,3-a]pyrimidine-5(4H)-one derivatives and evaluation of their anti-inflammatory activity. Lett Drug Des Dis 2015;13:141–8.
[37] Zhang T-Y, Li C, Li Y-R, Li X-Z, Sun L-P, Zheng C-J, Piao H-R. Synthesis and antimicrobial evaluation of aminoguanidine and 3-amino- 1,2,4-triazole derivatives as potential antibacterial agents. Lett Drug Des Dis 2016;13:1063–75.
[38] Zhang HJ, Zhang GR, Piao HR, Quan ZS. Synthesis and characterisation of celastrol derivatives as potential anticancer agents. J Enzyme Inhib Med Chem 2017;33:190–8.
[39] Shen QK, Deng H, Wang SB, Tian YS, Quan ZS. Synthesis, and evaluation of in vitro and in vivo anticancer activity of 14-substituted oridonin analogs: a novel and potent cell cycle arrest and apoptosis inducer through the p53-MDM2 pathway. Eur J Med Chem 2019;173:15–31.
[40] Luan T, Cao LH, Deng H, Shen QK, Tian YS, Quan ZS. Design and synthesis of C-19 isosteviol derivatives as potent and highly selective antiproliferative agents. Molecules 2018;24:121.
[41] De P, Baltas M, Bedos-Belval F. Cinnamic acid derivatives as anticancer agents-a review. Curr Med Chem 2011;18:1672–703.
[42] Li QF, Shi SL, Liu QR, Tang J, Song J, Liang Y. Anticancer effects of ginsenoside Rg1, cinnamic acid, and tanshinone IIA in osteosarcoma MG-63 cells: nuclear matrix downregulation and cytoplasmic trafficking of nucleophosmin. Int J Biochem Cell Biol 2008;40:1918–29.
[43] Ghosh AK, Brindisi M. Organic carbamates in drug design and medicinal chemistry. J Med Chem 2015;58:2895–940.
[44] Kamal A, Kumar BA, Suresh P, Juvekar A, Zingde S. Synthesis of 4beta-carbamoyl epipodophyllotoxins as potential antitumour agents. Bioorg Med Chem 2011;19:2975–9.
[45] Liu XK, Ye BJ, Wu Y, Lin ZH, Zhao YQ, Piao HR. Synthesis and anti-tumor evaluation of panaxadiol derivatives. Eur J Med Chem 2011;46:1997–2002.
[46] Wang Z, Li MY, Zhang ZH, Zuo HX, Wang JY, Xing Y, Ri M, Jin HL, Jin CH, Xu GH, Piao LX, Jiang CG, Ma J, Jin X. Panaxadiol inhibits programmed cell death-ligand 1 expression and tumour proliferation via hypoxia-inducible factor (HIF)-1alpha and STAT3 in human colon cancer cells. Pharmacol Res 2020;155:104727.
[47] Fan HY, Wang XK, Li X, Ji K, Du SH, Liu Y, Kong LL, Xu JC, Yang GQ, Chen DQ, Qi D. Curcumin, as a pleiotropic agent, improves doxorubicin-induced nephrotic syndrome in rats. J Ethnopharmacol 2020;250:112502.
[48] Yang Y, Guan D, Lei L, Lu J, Liu JQ, Yang G, Yan C, Zhai R, Tian J, Bi Y, Fu F, Wang H. H6, a novel hederagenin derivative, reverses multidrug resistance in vitro and in vivo. Toxicol Appl Pharmacol 2018;341:98–105.
[49] Jin HR, Jin SZ, Cai XF, Li D, Wu X, Nan JX, Lee JJ, Jin X. Cryptopleurine targets NF-kappaB pathway, leading to inhibition of gene products associated with cell survival, proliferation, invasion, and angiogenesis. PLoS One 2012;7:e40355.
[50] Dai ZC, Chen YF, Zhang M, Li SK, Yang TT, Shen L, Wang JX, Qian SS, Zhu HL, Ye YH. Synthesis and antifungal activity of 1,2,3-triazole phenylhydrazone derivatives. Org Biomol Chem 2015;13:477–86.
[51] Jia Z, Zhu Q. 'Click' assembly of selective inhibitors for MAO-A. Bioorg Med Chem Lett 2010;20:6222–5.
[52] Meldal M, Tornoe CW. Cu-catalyzed azide-alkyne cycloaddition. Chem Rev 2008;108:2952–3015.
[53] Abdel-Atty MM, Farag NA, Kassab SE, Serya RAT, Abouzid KAM. Design, synthesis, 3D pharmacophore, QSAR, and docking studies of carboxylic acid derivatives as Histone Deacetylase inhibitors and cytotoxic agents. Bioorg Chem 2014;57:65–82.
[54] Wilson WR, Hay MP. Targeting hypoxia in cancer therapy. Nat Rev Cancer 2011;11:393–410.
[55] Lei KF, Wu ZM, Huang CH. Impedimetric quantification of the formation process and the chemosensitivity of cancer cell colonies suspended in 3D environment. Biosens Bioelectron 2015;74:878–85.
[56] Zhou B, Zhan H, Tin L, Liu S, Xu J, Dong Y, Li X, Wu L, Guo W. TUFT1 regulates metastasis of pancreatic cancer through HIF1-Snail pathway induced epithelial-mesenchymal transition. Cancer Lett 2016;382:11–20.
[57] Umezu T, Tadokoro H, Azuma K, Yoshizawa S, Ohyashiki K, Ohyashiki JH. Exosomal miR-135b shed from hypoxic multiple myeloma cells enhances angiogenesis by targeting factor-inhibiting HIF-1. Blood 2014;124:3748–57.